Available online at www.sciencedirect.com
ScienceDirect
Combustion and Flame 149 (2007) 63–78
Combustion and Flame
www.elsevier.com/locate/combustflame

Modeling forest fire spread and spotting process with small world networks

Bernard Porterie [a,*], Nouredine Zekri [b], Jean-Pierre Clerc [a], Jean-Claude Loraud [a]

[a] *IUSTI/UMR CNRS 6595, Université de Provence, 5 Rue E. Fermi, 13453 Marseille cedex 13, France*
[b] *USTO, Département de Physique, LEPM, BP 1505 El Mnaouer, Oran, Algeria*

Received 22 December 2005; received in revised form 4 September 2006; accepted 8 December 2006

Available online 9 February 2007

Abstract

The small world network model is extended to study fire spread through forest fuels. The proposed model includes the short-range radiative and convective effects from the flame as well as the long-range "spotting" effect of firebrands. It uses a weighting procedure on network sites based on the characteristic times of thermal degradation and combustion of a flammable site. First the model is validated against nonspotting fire experiments in homogeneous media. It is then applied to heterogeneous media to illustrate its ability to provide realistic fire patterns. It is found that the concentration of flammable sites, p, is a good measure of local small world network properties. Front propagation exhibits two thresholds delimiting the spreading/nonspreading transition: the first corresponds to a geometric second-order phase transition line and is inversely proportional to the fire impact length, l_c, according to $p_c^{rn} = 0.5 l_c^{-1}$, and the second is a dynamic threshold resulting from the weighting procedure. The p-dependence of the fractal dimension of the burned area confirms the percolation transition line behavior. Second, firebrands are considered by introducing a characteristic spotting distance. For homogeneous systems, the effect of firebrands on spread rate and burned area is strengthened when the fire impact length decreases and the characteristic spotting distance increases. The head fire goes forward by jumps, especially for small values of the fire impact length. However, the development of spotfires can slow down the overall propagation process. For heterogeneous systems, spread rate and burned area are significantly reduced as the degree of disorder increases. The influence of firebrands then becomes weaker and smoother. The model underlines the existence of critical channels of the propagation cluster, allowing to stop the propagation of fire if they are cut off.

Keywords: Forest fire; Small world network; Fire spread; Percolation; Firebrands; Spotting

1. Introduction

Fire spread has been modeled for a long time using regular networks [1–5], as well as cellular automata [6–8], to include site weights. However, as suggested in 1976 by de Gennes [9], such networks did not take into account physical effects beyond the nearest

* Corresponding author.
E-mail address: bernard.porterie@polytech.univ-mrs.fr (B. Porterie).

0010-2180/$ – see front matter
doi:10.1016/j.combustflame.2006.12.008

Nomenclature

CFL	Courant–Friedrich–Levy
D	fractal dimension of the burned area
D_0	characteristic spotting distance
h	ratio of impact parameters for a binary system
l_x, l_y, l_c	impact parameters
L	size of the square network
M	average mass proportion of burned sites during fire propagation
N_{bs}	number of burning sites
N_{fb}	number of firebrands generated in the system
n_c	number of time steps required for the combustion of an active site, $t_c/\delta t$
n_{TD}	number of time steps required for the thermal degradation of an active site, $t_{TD}/\delta t$
p	density of active sites
p_c	percolation threshold
ros	rate of spread of the head fire
rn	regular network
R	dynamic propagation threshold, t_c/t_{nn}
swn	small world network
t_c	characteristic time of combustion of an active site
t_{TD}	characteristic time of thermal degradation of an active site
t_{nn}	time required for the nearest neighbor of a burning site to reach ignition

Greek symbols

δt	time step
δl	lattice parameter
ξ	correlation length, defined as the largest cluster size for heterogeneous systems

Subscripts and superscripts

bs	burning sites
fb	firebrands
nn	nearest neighbor
rn	regular network
swn	small world network
TD	thermal degradation

neighbors of a burning site, such as flame-induced radiative/convective effects or firebrand impact. There is some evidence that models with local contacts only do not mimic real fires well [10]. Long-range connections were recently modeled by a small world network (swn) [11] having the main properties of a social network, i.e., the clustering (a cluster is defined as a group of interconnected active sites) and possible connections between any two sites in the network within a finite number of steps. This model seems to fit very well many forms of social behavior such as epidemics. It is built from a regular network (rn), but in addition to the number k of nearest neighbors, ϕ long-range connections per site are randomly introduced throughout the whole network. Let the control parameter be the density of the network sites, p, participating in the propagation process in heterogeneous systems. There is a percolation-type threshold value, p_c^{swn}, corresponding to the appearance of a cluster whose size behaves as a power law with $p - p_c^{swn}$ [12,13]. This threshold was extensively investigated for 1D systems and its dependence on k and ϕ satisfies the following equation [14,15]:

$$\phi = \frac{(1 - p_c^{swn})^{k/2}}{p_c^{swn}}. \tag{1}$$

The exponent $k/2$ refers to the number of neighbors in the propagation direction. In the case of epidemics, this threshold corresponds to the smallest concentration of "susceptible individuals" leading to the disease outbreak [14]. In the case of fires, this is the smallest density of forest fuel elements delimiting the spreading/nonspreading transition. It is worth noting that this threshold must be distinguished from that of regular networks (p_c^{rn}), where the largest cluster connects the two ends of the system or diverges for infinite-size systems [4]. Furthermore, systems such as airport networks require, in addition to long-range connections, the introduction of weights either in their nodes (airports) or links (planes) [16]. To correctly model fire propagation through a network of forest fuel elements, long-range connections corresponding to fire and firebrand impacts have to be considered, as well as weights due to thermal degradation and combustion processes. Fire spread is mainly dependent on the characteristic lengths of fire impact and on the spotting distance. This leads, in our model, to the definition of impact parameters beyond the nearest neighbors.

Spotting is the process whereby flaming or burning embers (firebrands) produced when brush and trees burn rapidly are lofted by the fire plume and transported downwind to start new fires (spotfires) in receptive fuel beds, including forests and houses ahead of the main fire. This is the dominating fire propagation mechanism in high-intensity forest fires. Firebrands (e.g., bark, needles, leaves, cones, and small branches) may give rise to secondary fires hun-

dreds of meters from the fire front and are the primary cause of house ignition in wildland–urban interface areas. Spotting dramatically alters fire growth patterns and behavior and makes fire suppression much more difficult. On 20 October 1991 the Oakland/Berkeley Hills fire quickly overwhelmed the initial attack fire crew, in part due to firebrand propagation and spotting hundred of meters ahead of the main front [17]. The factors that affect the generation and propagation of firebrands are fuel (size, type, moisture content, arrangement), weather, and topography. Crown fires can be excellent generators of embers for spotting. Although lofting and propagation of burning brands in forest fires have received considerable attention ([18–23], to name but a few), very little research has been conducted to study the role of firebrands on the propagation of the fire itself. To our knowledge, the only study that attempts to estimate such influence is that of Hargrove et al. [24], who used a broad-scale probabilistic model of forest fires burning through heterogeneous landscapes. However, the model considers fire propagation as a diffusive spread from each ignited cell to any of the nearest neighbors, and firebrands often fall near the cell that generated them, which prohibits creating distinct fires in the conventional sense.

In this paper a two-dimensional model based on a weighted-site small world network is presented to study fire spread through homogeneous and heterogeneous forest fuel beds. First the model is described and results are compared with experimental data in homogeneous fuel beds for different fire conditions. The effects of wind and slope on the rate of spread (ros) are investigated. The model is next applied to heterogeneous media, and propagation properties such as propagation thresholds and fractal dimension of the average burned area are studied. The model is then extended to show how fire behavior is affected by firebrands.

2. Model description

The present model is based on the small world network (swn) initially proposed by Watts and Strogatz [11]. It is built from a square lattice of size L. The concept of short-range connections (k) in the standard swn is here replaced by that of impact parameters defining the influence zone of a burning site (Fig. 1). This means that for a given burning site, its influence zone is characterized by one (isotropic propagation) or two impact parameters (as a result of wind or/and slope effects) in such a way that all active sites present in this zone are connected to the burning site. The impact parameters can be either identical to the characteristic lengths l_x and l_y directly related to the radiative/convective impact of the burning site (deterministic case) or generated following a Poisson-like distribution based on these lengths (random case) [25]. They are dependent on fire and fuel conditions and expressed in an arbitrary length unit (δl) corresponding to the lattice parameter (Fig. 1). A high value of the impact parameter ratio l_y/l_x corresponds to a strong anisotropy of the front shape induced by the terrain slope and/or wind effects in the y-direction. In the absence of firebrand generation, the present model can be considered as a regular network for the whole system, whereas it is regarded as a swn on a local scale [26,27]. Long-range connections correspond to the transport of firebrands from burning sites beyond the influence zone (Fig. 1). It has been observed from experiments [28] and shown from a fine-scale physically based deterministic model [29] that in most fire situations the density of firebrands on the ground decreases exponentially with the distance from the fire front. This negative exponential distribution law was also used in the SPOT subroutine of the BEHAVE fire prediction model [30]. The spotting effect of firebrands is simulated by permitting each burning site to generate a time-dependent number of firebrands, $N(t)$, depending on fuel type. When a firebrand lands on an unburned site, an ignition probability, $P_i(t)$, based on the moisture content and the type of the receptive fuel material, is used to determine whether the firebrand causes a new fire to start [24]. Such a firebrand is called efficient. To account for variations in wind direction, firebrands travel downwind in a 60° random angle around the prevailing wind direction.

The maximum number of efficient firebrands generated in the L-size system is

$$N_{\mathrm{fb}}(t) = cN_{\mathrm{bs}}\left[1 - \exp(-L/D_0)\right] \tag{2}$$

with

$$c = \frac{1}{t_{\mathrm{c}}} \int_0^{t_{\mathrm{c}}} N(t) P_i(t)\, \mathrm{d}t. \tag{3}$$

The present model uses a weighting procedure on sites based on the knowledge of two characteristic times, namely the time of thermal degradation of a flammable site, t_{TD}, and that of combustion, t_{c}. The state of advancement of thermal degradation and combustion processes is performed at each time step δt, taken here as the arbitrary time unit. After ignition, a given site needs n_{c} time steps to burn completely, according to $t_{\mathrm{c}} = n_{\mathrm{c}} \times \delta t$, whereas a site located at the limit of the influence zone of a burning site (i.e., at a distance l_{c} from this site, where l_{c} is elliptically dependent on l_x and l_y as shown in Fig. 1b) needs n_{TD} time steps to reach ignition ($t_{\mathrm{TD}} = n_{\mathrm{TD}} \times \delta t$).

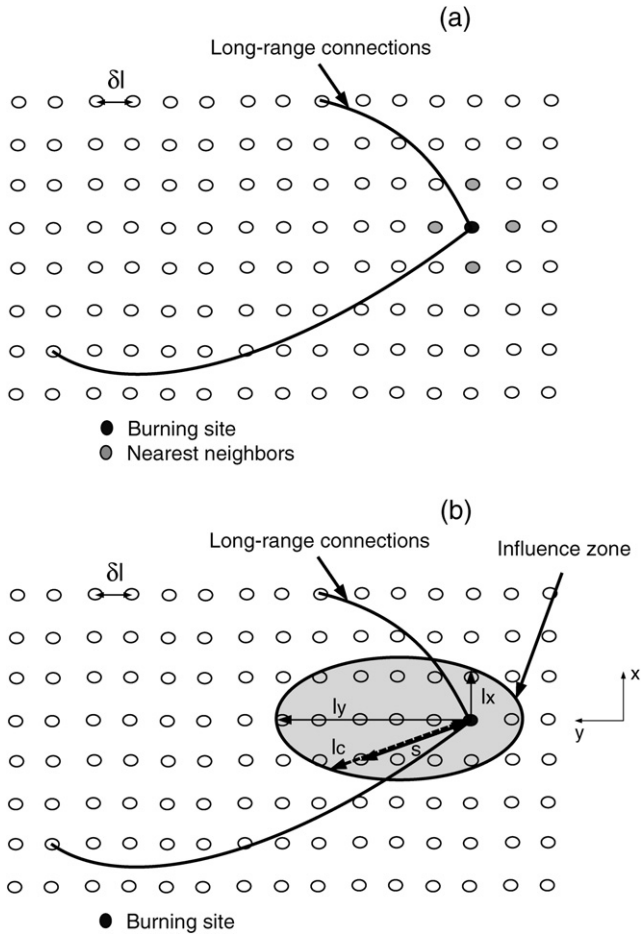

Fig. 1. The standard swn (a) is built from a regular square lattice. In the present swn (b) the nearest neighbors of a burning site are replaced by the influence zone of the burning site. Long-range connections are due to firebrands. δl is the lattice parameter.

A fire-exposed site located at a distance s from the burning site needs $n(s)$ time steps to reach ignition. There is an evidence from experimental observations that the degradation time increases sharply with increasing distance s. An exponential dependence is here assumed, which leads to

$$n(s) = (n_{\mathrm{TD}})^{s/l_c}. \tag{4}$$

The initial degradation level of this site is then $n_{\mathrm{TD}} - n(s)$. At each time step, its degradation level increases by one unit until ignition. If this site is exposed to two or more burning sites, its initial degradation level is $n_{\mathrm{TD}} - n(s_i)$, where s_i is the distance to the nearest burning site, whereas each of the other burning sites contributes one unit. As the unit time step is arbitrary, the number of levels is determined from the characteristic thermal degradation and combustion times of the fuel material. However, the CFL-like condition $n_{\mathrm{TD}} > 1$ is required to avoid the burning of the influence zone in one time step. Otherwise, from Eq. (4), $n_{\mathrm{TD}} = 1$ leads to $n(s) = 1$, which corresponds to a physically unrealistic situation where the radiative/convective impact is independent of the distance from the burning site.

Fuel type and moisture content do not affect the weighting procedure, whereas the influence zone should be modified as well as the characteristic times of thermal degradation and combustion.

2.1. Homogeneous and heterogeneous media

For homogeneous media the forest fuel elements that totally cover the system are of the same kind. Heterogeneity means the existence of two or more fuel types in the system (e.g., different species, or the same species with different moisture content), thus leading to different behavior under fire. For a binary system composed of sites A and B uniformly and randomly distributed in the system, it is convenient to define the proportion of sites belonging to each of them as p

and $1-p$, respectively, as well as the impact parameters in the propagation direction, l_A and l_B, with the arbitrary condition $l_B \leqslant l_A$ (the impact parameter ratio l_y/l_x is the same for both kinds of sites). The characteristic times for thermal degradation and combustion are assumed to be the same for both fuel types. For homogeneous media $h = l_B/l_A$ is equal to 1, independently of p. The level of heterogeneity is then defined by the knowledge of $p \neq 1$ and of the impact parameter ratio $h < 1$. In the limit of a total heterogeneity, $h = 0$, the system consists of p occupied sites with an impact parameter l_A; the remaining $1-p$ sites correspond to nonflammable areas such as rock, roads, and water ($l_B = 0$).

2.2. Dynamic and percolation thresholds

Let us now consider the dynamic aspect of the swn model. The thickness of the fire area is defined as the distance covered by the fire during the combustion time t_c. Defining t_{nn} as the time required for the nearest neighbor to reach ignition, directly related to t_{TD} ($t_{nn} = n(1) \times \delta t$, with $n(1)$ given by Eq. (4)), a propagation parameter for a single burning site can be expressed as

$$R = \frac{t_c}{t_{nn}}. \tag{5}$$

Fire spread occurs for $R \geqslant R_c$, where R_c is the dynamic propagation threshold. In the case of a single burning site, $R_c = 1$. For multiple burning sites (characteristic of real fire fronts) it was found that the threshold value is smaller than one [27]. This will be discussed below in order to complete the study. In the applications below the condition $R > 1$ is satisfied, which ensures that far from the dynamic threshold a burning site will continue to burn before the nearest neighbor ends its thermal degradation phase and burns in turn. For spotting fire conditions, the afterlanding combustion time of an efficient firebrand is assumed to be longer than that of the thermal degradation of the receptive material ($R > 1$).

Totally heterogeneous systems are characterized by two geometric propagation (percolation) thresholds: that of a regular network, p_c^{rn}, and that of the swn in the sense of Newman and Watts [15], p_c^{swn}. In both cases various clusters are randomly distributed in the system. In the case of regular networks ($p \gtrsim p_c^{rn}$), propagation reaches the opposite side of the network and the largest cluster size diverges for infinite-size systems. For the standard swn model, where long-range connections are included ($p \gtrsim p_c^{swn}$), the largest cluster size, ξ, starts increasing as a power law above this threshold $\xi = (p - p_c^{swn})^x$, x being a positive real number [12]. This power-law behavior represents the increase in the mass fraction burned.

2.3. Characteristic lengths

Three different characteristic lengths are involved in the propagation process: the impact parameter l_c, the spotting distance D_0, and the correlation length ξ.

- For nonspotting fire conditions, propagation is characterized by the influence zone of a burning site. For systems located within the influence zone, fire propagation is independent of the size of the system, which suggests a ballistic propagation (i.e., fire propagates from one side of the system to the other independently, as if it is not aware of the presence of the other sites). Otherwise propagation is diffusive.
- The distance traveled by a firebrand is generated according to an exponentially decaying probability distribution based on the characteristic spotting distance D_0 [28,29]. From Eq. (2), two asymptotic behaviors of this probability appear, depending on the size of the system:

$$D_0 \gg L, \quad N_{fb}(t) = cN_{bs}(t)\frac{L}{D_0} \tag{6}$$

and

$$D_0 \ll L, \quad N_{fb}(t) = cN_{bs}(t). \tag{7}$$

Clearly, a size effect appears for large spotting distances compared with L while the number of firebrands saturates for very small spotting distances. For infinite-size systems, the total probability reaches a maximum since all firebrands will fall within the system. It is then easy to understand the interest forest managers may have in the compartmentation of forest lands to reduce the spotting effect.

- For completely heterogeneous systems ($h = 0$), clusters of different sizes appear. The largest cluster size (correlation length) depends on the density of active sites, p. For system sizes greater than the correlation length, ξ, finite size effects do not occur around p_c^{rn} [4]. Above p_c^{rn}, the largest cluster size diverges and propagation resembles that in homogeneous systems. Below p_c^{swn}, $\xi = 0$ which corresponds to a nonspreading condition. For $p_c^{swn} < p < p_c^{rn}$ the largest cluster size is finite and a competition appears between ξ and D_0. The above analysis remains valid if one replaces the size of the system, L, with ξ in such a way that for $\xi \ll D_0$ the probability is high that firebrands will fall in inactive zones. In contrast, for $\xi \gg D_0$, firebrands will fall in the largest cluster, which in turn enhances the propagation process. A saturation effect of the area burned will then occur.

It may be noted that for nonspotting fire propagation, the concentration of remaining active sites is constant during propagation, while the spotting process causes the proportion of active sites to decrease with time, which in turn corresponds to a dynamic percolation and can lead to a slowing down of fire spread. Such behavior contrasts with that of electrical networks where the sites remains active during propagation [31].

3. Results and discussion

In this section, two different propagation processes in homogeneous or heterogeneous systems are investigated: nonspotting and spotting fire spread. A square network of 300 × 300 sites is used, which is sufficient to avoid finite-size effects for the nonspotting systems considered [27]. Active sites in heterogeneous systems are uniformly and randomly distributed. Arbitrary units are used below, with the exception of the model validation section which requires physical units.

3.1. Nonspotting fire spread

3.1.1. Homogeneous media ($h = 1$): model validation

The aim of this section is to compare swn model results with the laboratory-scale fire experiments carried out by Mendes-Lopes et al. [32] and Dupuy [33]. Point ignition was considered and the fuel bed was composed of pine needles (*Pinus pinaster*). First, the impact parameters of the model were determined by estimating the radiative impact from the view factor for elementary flames. The correlations of Putnam [34] and Albini [35] were used to determine the geometric properties of the flame (height and angle) for the experimental conditions (wind, slope, and fuel). The square network used corresponds in the present situation to a physical domain of 1 × 1 m. Thus the lattice parameter is $\delta l = 0.33$ cm. For no-slope and no-wind conditions, the estimated impact parameter is $l_c = 3\delta l = 1$ cm. The characteristic times of combustion and thermal degradation of pine needles are $t_c = 30$ s and $t_{TD} = 100$ s. For a time step $\delta t = 1$ s the corresponding numbers of levels are $n_c = 30$ and $n_{TD} = 100$. The l_c-dependence of the rate of spread of the fire is illustrated in Fig. 2 and shows power-law behavior with a slower spreading for a randomly generated value of l_c. The rate of spread is given by ros (cm/s) $= 0.102 l_c^{1.51}$ for a deterministic impact parameter while it varies as ros (cm/s) $= 0.080 l_c^{1.47}$ if this parameter is randomly generated. Negligible statistical fluctuations of the ros are found in the random case. On flat terrain with no wind, the fire perimeter should maintain a circular shape centered at the ignition point. This is shown in Fig. 3 after 144 s of fire propagation for an impact parameter $l_c = 1$ cm. Good agreement with experimental data is observed in the random case, while in the deterministic case the area burned by the fire is overestimated. The same conclusions can be drawn for the 30°-upslope conditions, where the impact parameters are estimated to be $l_x = 3\delta l = 1$ cm and $l_y = 7\delta l = 2.33$ cm. This is shown in Fig. 4, which exhibits the elliptic fire perimeter 78 s after point ignition.

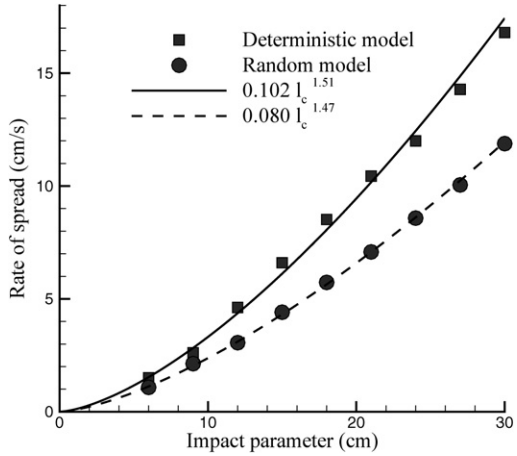

Fig. 2. Rate of fire spread vs the impact parameter.

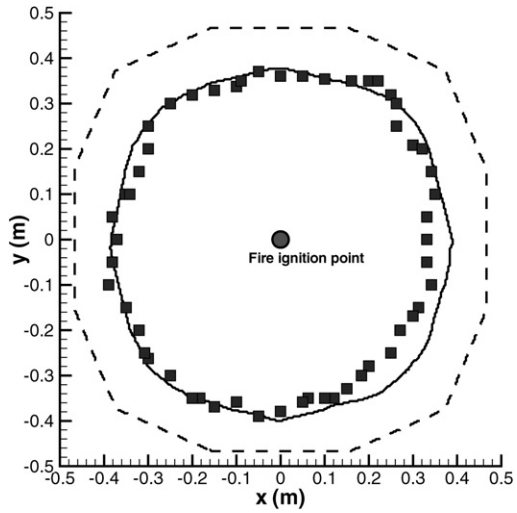

Fig. 3. Fire perimeters for a flat terrain in no-wind conditions 144 s after point ignition. The dashed line corresponds to model results with a fixed characteristic length of $l_x = l_y = 1$ cm. The solid line corresponds to model results with a randomly generated impact parameter. The experimental fire perimeter [33] is represented by symbols.

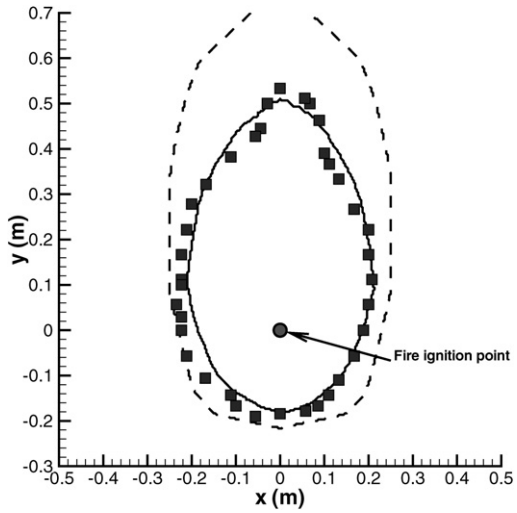

Fig. 4. Fire perimeters for a 30°-upslope terrain with no wind 78 s after point ignition. The dashed line corresponds to model results with fixed characteristic lengths: $l_x = 1$ cm and $l_y = 2.33$ cm. The solid line corresponds to model results with randomly generated impact parameters. The experimental fire perimeter [33] is represented by symbols.

The influence of wind speed on the ros of the head fire is given in Fig. 5. The variation in the slope of the ros as a function of wind, which corresponds to the transition from a buoyancy-dominated to a wind-dominated regime [36], is well reproduced by the present model. As discussed above, a dynamic propagation threshold exists and corresponds to $R_c = 1$ for a single burning site. This threshold is expected to be smaller than one for line-fire propagation, since a site can be the nearest neighbor of more than one burning site, which in turn leads to an increase in its rate of thermal degradation. This is clearly seen in Fig. 6, where the ros is plotted versus R assuming a constant value of t_{nn} (see Eq. (5)). The dynamic transition occurs for a threshold value $R_c \approx 0.5$, whatever the impact parameter. Fig. 6 shows that, beyond a certain value of R or t_c, the whole of the influence zone contributes to the propagation process. Fire then propagates at a maximum ros. For any system larger than the influence zone, ros is not size-dependent [27].

From numerical experiments, it was found that the computational (CPU) time required to simulate the fire propagation from one side to the opposite side of the system is nearly proportional to the square of network size. Moreover, it can be significantly smaller than the real time (estimated by multiplying the number of steps by the time step). For impact parameters $l_x = 2\delta l$ and $l_y = 6\delta l$, the time for fire propagation corresponds to 148 time steps. This takes about 72 s of CPU time on a Pentium 4 3.06 GHz processor. For example, when the distance between forest trees is $\delta l = 3$ m and assuming that the time for the nearest neighbor to ignite is about $t_{nn} = 25$ s, the 100-level degradation process leads to a time step of 12 s (from Eq. (4)), which indicates that the ratio of real time to CPU time is about 25. This gives a somewhat-realistic ros of 0.51 m/s.

3.1.2. Heterogeneous media ($h = 0$)

The model is applied here to heterogeneous media composed of p active sites and $1 - p$ inactive or non-flammable sites ($h = 0$) for $l_x = 3\delta l$ and $l_y = 7\delta l$. Fig. 7 shows the areas involved in fire spreading after $78\delta t$ on a 30°-upslope terrain with no wind for values of p above p_c^{rn}, which are $p = 0.3$ and 0.5. The difference in fire behavior can be explained by the predominance of the local swn effect on the rn effect for

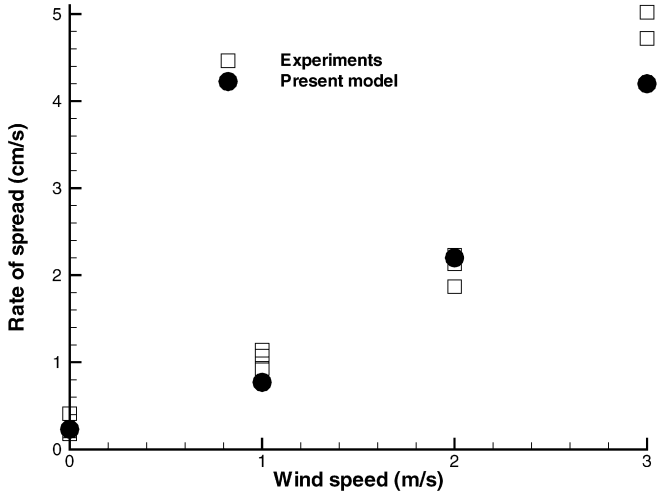

Fig. 5. Rate of fire spread vs wind speed.

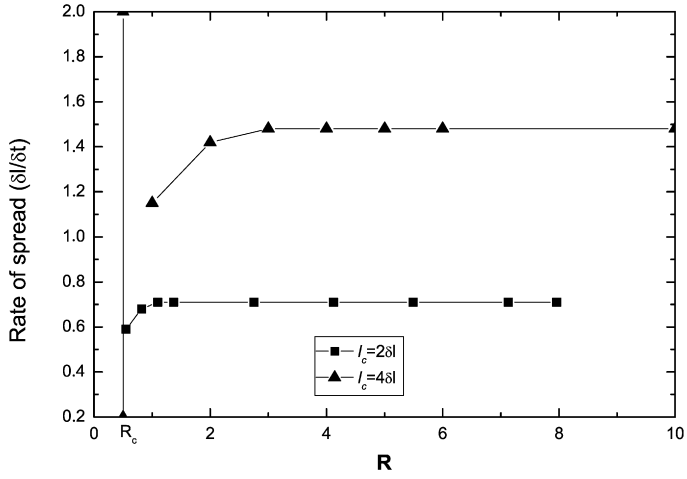

Fig. 6. Rate of fire spread vs R for different impact parameters.

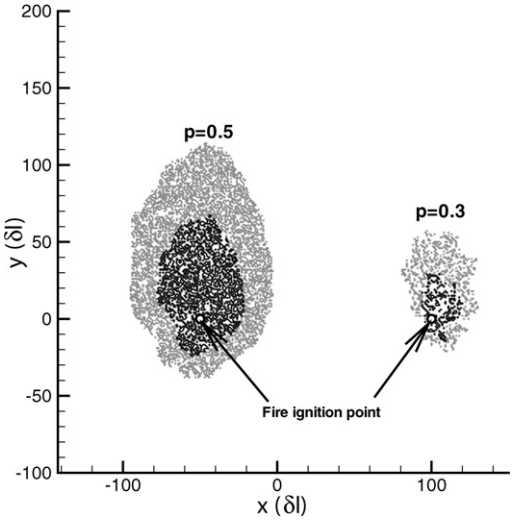

Fig. 7. Fire patterns $78\delta t$ after point ignition for densities of active sites $p = 0.5$ and $p = 0.3$. Impact parameters are randomly generated with $l_x = 3\delta l$ and $l_y = 7\delta l$. The black zones correspond to the burned area, the gray to the burning area, and the white zone inside the fire perimeter corresponds to inactive sites. For both cases, $t_{TD} = 100\delta t$ and $t_c = 30\delta t$.

$p = 0.3$. This can lead to the formation of fire fingers or dead branches on fire edges. For small concentrations of active sites ($p = 0.3$ in Fig. 7), the fragmented front structure appears as a ballistic propagation. For higher values of p, the propagation becomes mainly diffusive ($p = 0.5$ in Fig. 7), the regular network effect being dominant. Between ballistic and diffusive regimes, a crossover can occur, as observed by Sapoval et al. [37]. Next the spreading/nonspreading transition threshold is examined by varying p. A statistical averaging process is carried out by igniting the first line of sites (300 sites) instead of a single site. This process provides the average time and rate of spread as well as the average mass M (proportion) of burned sites during fire propagation. For simplicity, let us consider an isotropic propagation process (i.e., $l_x = l_y = l_c$). The p-dependence of the average burned mass and fire propagation duration are shown in Fig. 8 for $l_c = 2\delta l$. This figure shows the usual second-order phase transition observed in regular networks [4], namely the cluster divergence at p_c^{rn} (Fig. 8a) and the sharp change of mass behavior. The mass M corresponds to the probability of belonging to the largest cluster. This second-order phase transition, which reveals the regular network properties of the system, is observed for any value of the impact parameter. The effect of the impact parameter on the value of the percolation threshold is shown in Fig. 9. The regular network percolation threshold, p_c^{rn}, appears as a power-law function of the impact parameter l_c with an exponent -1 showing a transition line. If connections are restricted to the nearest neighbors ($l_c = \delta l$) the known bond percolation threshold for a square regular network, $p_c^{rn} = 1/2$, is reproduced by the power-law fitting function. From a physical point of view, this demonstrates that radiative and convective effects from the flame (including the effects of slope inclination and wind through the impact parameter) modifies the dynamics of propagation as well as the value of the propagation/nonpropagation threshold. The scaling behavior of the second-order phase transition can be examined by means of the fractal dimension, which is defined as the exponent, D, of the power-law decay function of the burned area, M, as a function of the system size: $M \propto L^{D-2}$. Line ignition ensures that propagation takes place since at least one of the initial

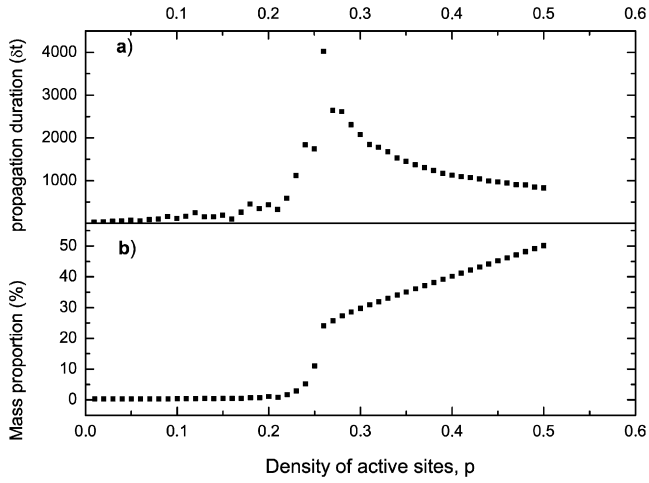

Fig. 8. (a) Fire propagation duration and (b) burned mass proportion M vs concentration p. $l_c = 2\delta l$, $t_{TD} = 100\delta t$, and $t_c = 30\delta t$.

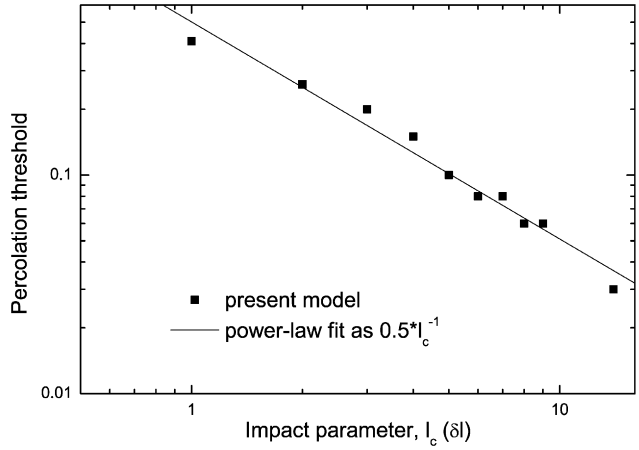

Fig. 9. Percolation threshold p_c vs impact parameter l_c. (—) is a power-law fit of swn values. $t_{TD} = 100\delta t$ and $t_c = 30\delta t$.

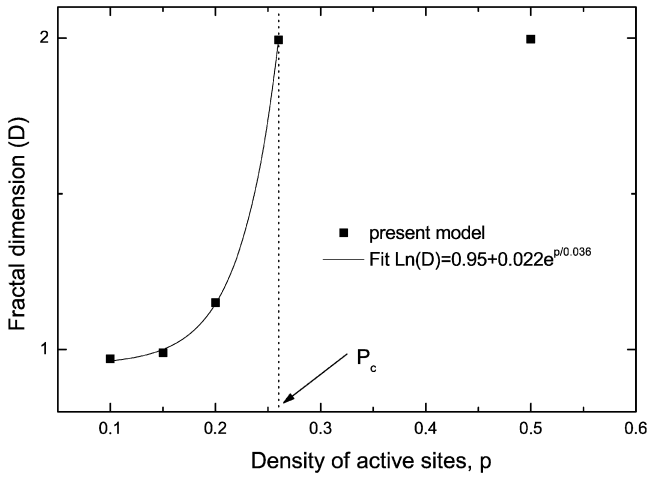

Fig. 10. Fractal dimension of the area covered by the fire vs concentration p. Here, $l_c = 2\delta l$, $t_{TD} = 100\delta t$, and $t_c = 30\delta t$. The dotted line corresponds to the percolation threshold p_c. The solid line is a fit of swn values.

sites belongs to the largest cluster. Moreover, other sites which belong to other clusters may contribute to propagation. Fig. 10 shows the p-dependence of the fractal dimension for an impact parameter $l_c = 2\delta l$, which corresponds to $p_c^{rn} \approx 0.26$. Above this threshold, the burned area covers the whole system and $D = 2$. Below this threshold, the propagation covers only a part of the system and $D < 2$. It is worth noting that in the limit of $p = 0$, the value of D tends to 1 which corresponds to the fractal dimension of the ignition line. The transition shown in Fig. 10 between the p-dependence of the fractal dimension below p_c^{rn} and its nondependence above p_c^{rn} has previously been observed for aggregates (diffusion-limited aggregation, DLA) [37] as well as in a reaction diffusion model [38]. At about p_c^{rn} the mass does not behave as a power-law function of the size. This means that the burned area becomes multifractal at the percolation threshold as a result of the random generation of the impact parameter. Self-similar behavior has been obtained by Albinet et al. [1] assuming only deterministic cases of fire front propagation. For such cases, we found an overestimation of the rate of spread.

3.2. Spotting process

This section deals with the eclosion and the growth of a point-ignited fire. Propagation takes place in homogeneous and heterogeneous forest fuel media. For heterogeneous systems, the location of the furthermost burning site and the burning area are averaged over 100 realizations, taking into consideration the size of the systems studied. A burning site can belong either to the primary fire front or to a secondary fire generated by spotting. Very little information exists for estimating parameters describing the spotting process. This led Hargrove et al. [24] to estimate an arbitrary but consistent set of parameters for lodgepole pine as forest fuel. For very dry weather conditions (see Table 2 in [24]), the value of c calculated from Eq. (3) is $c = 1.02/t_c$.

3.2.1. Homogeneous media

Nonspotting and spotting fire propagation with $D_0 = 30\delta l$ and $90\delta l$ are compared in Fig. 11 for two different instants. This figure illustrates the eclosion and development of secondary fires and their absorption by the primary front. When the spotting distance increases, the burning area increases and becomes more structured. Long-range spotting gives rise to secondary fires that develop considerably before being absorbed into the primary front. Fig. 12 shows the time evolution of the number of burning trees, N_{bs}, for different values of the spotting distances D_0 and of the impact parameter l_y. The burning area increases with the spotting distance and a maximum appears. Such behavior is similar to that observed in predator–prey and epidemic models [39]. For nonspotting fire propagations ($D_0 = 0$ in Fig. 12), the number of burning trees, N_{bs}, increases linearly with time until the primary front reaches the opposite end of the system. For spotting fire propagations and $D_0 \ll L$ ($D_0 = 30$ and $90\delta l$ in Fig. 12), N_{bs} seems to increase exponentially. This results from the time variation of N_{bs}, which is proportional to N_{fb}, according to Eq. (7). For a small value of the impact parameter $l_y = 4\delta l$, fire propagates slowly and allows secondary fires to develop before absorption. The influence of firebrands on N_{bs} is then relatively more pronounced. However, for small values of D_0, firebrands can fall close to the primary front. This front reaches an area that is already burned, and this causes the time increase of N_{bs} to slow down, as shown in Fig. 12a for $D_0 = 30\delta l$ around $t = 150\delta t$. The influence of firebrands starts to appear early when the number of burning sites becomes large enough to give rise to a secondary fire. This is more easily done with a high value of the impact parameter, as shown in Fig. 12. By comparing the time evolution of the furthermost position of the front (Fig. 13) for spotting and nonspotting fire propagations, it appears that spotfires lead to a significant increase in the ros with successive jumps. This swn effect is all the more pronounced for large values of the spotting distance since the primary fire propagates more slowly allowing the secondary fires to develop. One can expect that, for $D_0 \gg L$, the swn effect corresponds to spotting from one side of the system to the other.

3.2.2. Heterogeneous media

As indicated above, h is the parameter that defines the degree of heterogeneity. It varies from $h = 0$ (totally heterogeneous systems) to $h = 1$ (homogeneous systems) via $h = 0.5$, where an A site has an impact parameter that is twice that of a B site. Fig. 14 represents fire patterns for these values of h and a spotting distance of $D_0 = 90\delta l$ at two different instants. The impact parameters are $l_x = 2\delta l$ and $l_y = 6\delta l$. From a comparative examination of Figs. 14a–14d, it is found that both primary and secondary fires develop more rapidly in homogeneous media. This gives a larger number of burning sites, which in turn leads to a more pronounced firebrand effect on propagation. Through a completely heterogeneous medium (Figs. 14e and 14h, where $h = 0$), propagation is significantly slowed down. The uniformly distributed inactive zones appear clearly after the passage of the fire. This can lead to unburned "islands" inside the fire perimeter, unlike homogeneous systems, where compact clusters are obtained. Such lacunarity (i.e., the void distribution inside the cluster) has been observed in real wildfires from the areas of burned sur-

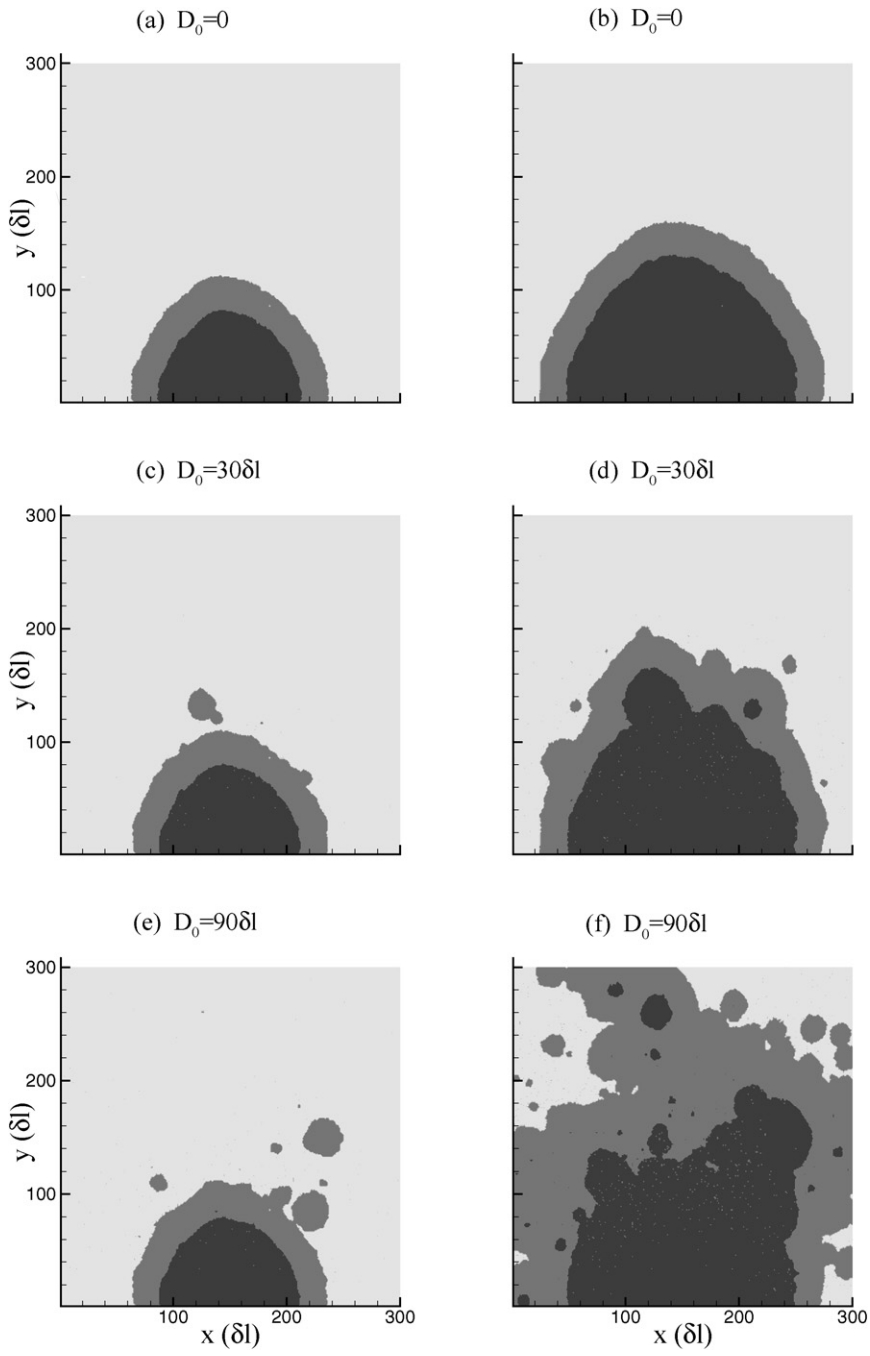

Fig. 11. Fire patterns, $120\delta t$ (left-hand column) and $170\delta t$ (right-hand column) after point ignition, for nonspotting and spotting fire propagations with characteristic spotting distances $D_0 = 30$ and $90\delta l$. The gray area corresponds to the burning zone and the black area to the burned zone. Point ignition occurs at $x = 150\delta l$ and $y = 0$. Here, $l_x = 3\delta l$, $l_y = 4\delta l$, $t_{\mathrm{TD}} = 100\delta t$, and $t_{\mathrm{c}} = 30\delta t$.

face estimated by satellite imagery [40]. The spotting process is considerably reduced, as the firebrands are fewer and can fall in nonflammable zones. Figs. 14g and 14h correspond to a completely heterogeneous system ($h = 0$) with a concentration $p = 0.5$, which is above the percolation threshold of regular networks (rn) and a fortiori above the swn threshold ($p > p_{\mathrm{c}}^{\mathrm{rn}} > p_{\mathrm{c}}^{\mathrm{swn}}$) [15]. However, they could illus-

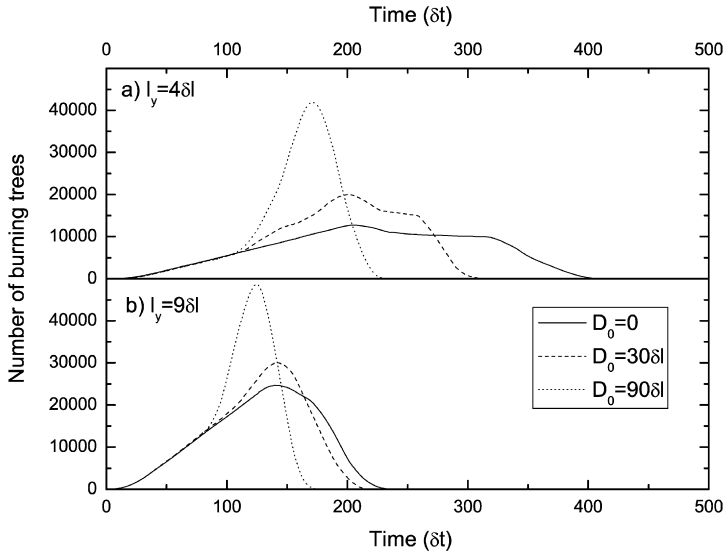

Fig. 12. Time evolution of the number of burning sites for nonspotting and spotting fire propagations with characteristic spotting distances $D_0 = 30$ and $90\delta l$. (a) $l_y = 4\delta l$ and (b) $l_y = 9\delta l$. For all cases: $l_x = 3\delta l$, $t_{\mathrm{TD}} = 100\delta t$, and $t_{\mathrm{c}} = 30\delta t$.

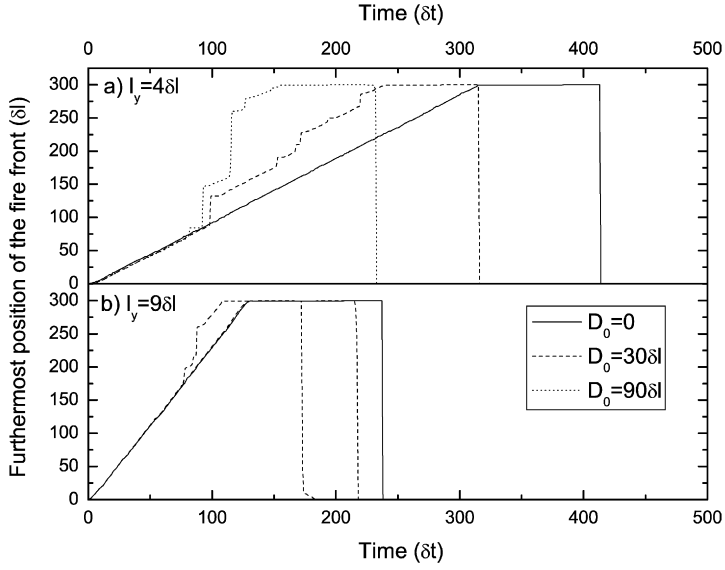

Fig. 13. Time evolution of the furthermost position of the fire front for nonspotting and spotting fire propagations with characteristic spotting distances $D_0 = 30$ and $90\delta l$. (a) $l_y = 4\delta l$ and (b) $l_y = 9\delta l$. For all cases: $l_x = 3\delta l$, $t_{\mathrm{TD}} = 100\delta t$, and $t_{\mathrm{c}} = 30\delta t$.

trate different p-dependent configurations after a fire. Fig. 14h corresponds to a typical rn fire pattern for $p > p_{\mathrm{c}}^{\mathrm{rn}}$. Fig. 14g could correspond to an swn fire pattern for $p > p_{\mathrm{c}}^{\mathrm{swn}}$, as the burned area is large enough, as well as a rn behavior for $p < p_{\mathrm{c}}^{\mathrm{rn}}$, as the primary front stops before reaching the opposite side.

Figs. 15 and 16 represent the time evolution of the burning mass and of the furthermost burning tree for different degrees of heterogeneity. It appears that the action of firebrands decreases with h. The presence of B sites ($h = 0$ and $h = 0.5$) increases the difficulty spotfires have in developing and decreases the probability of spotting (Fig. 15). The firebrand effect on fire propagation is then lessened, as shown in Figs. 16a and 16b. It may be noted that in Fig. 16a the average head fire does not reach the opposite side of the system, whatever the spotting distance, unlike in the binary case ($h = 0.5$), where fire propagates for all sample configurations. Since the present model can be viewed as a regular network for nonspotting systems,

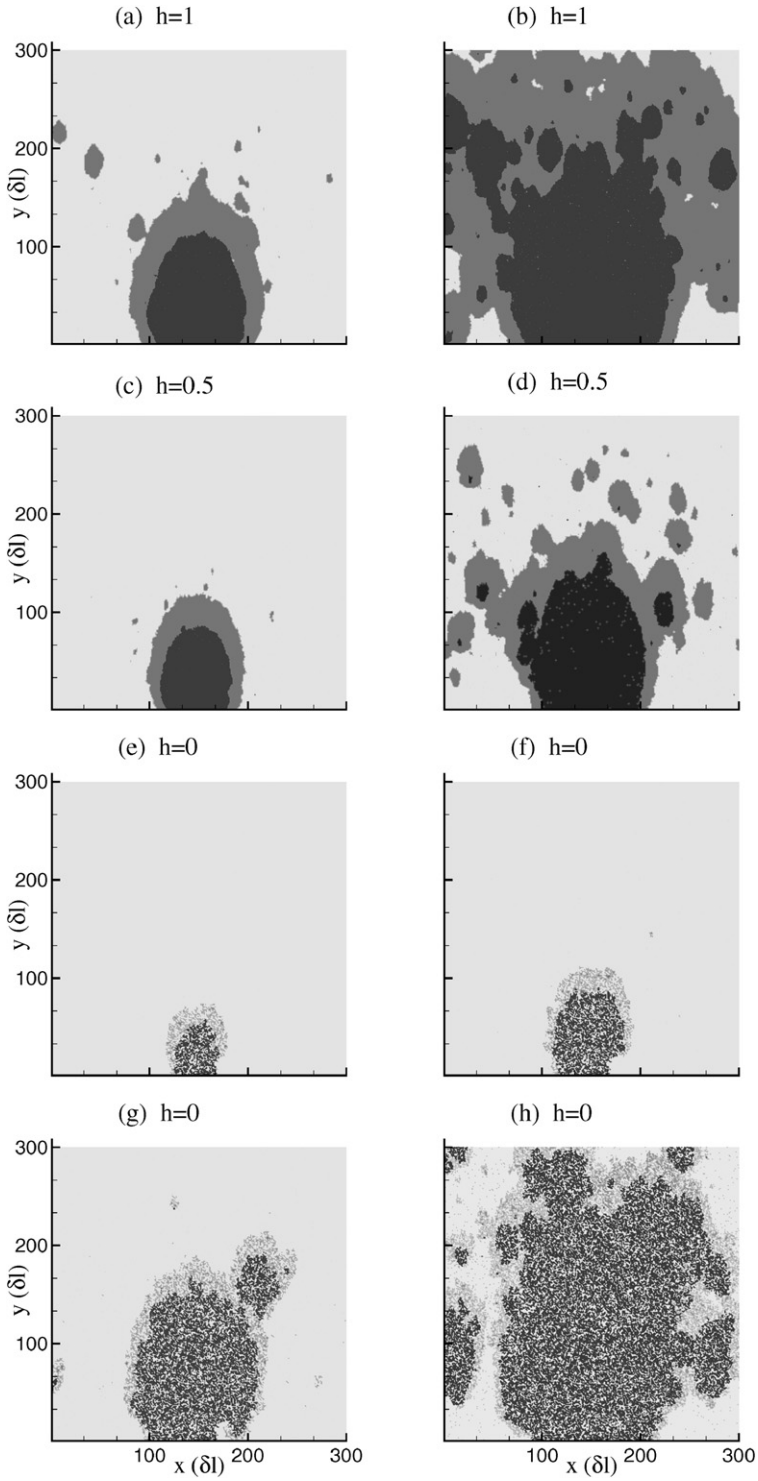

Fig. 14. Diagrams (a)–(f): fire patterns, $125\delta t$ (left-hand column) and $175\delta t$ (right-hand column) after ignition, for a characteristic spotting distance $D_0 = 90\delta l$ and different degrees of heterogeneity, h. Diagrams (g) and (h): fire patterns, respectively, at $270\delta t$ and $370\delta t$ after ignition, for $D_0 = 90\delta l$ and $h = 0$. Note that diagrams (c)–(h) correspond to 50% inactive sites. The gray area corresponds to the burning zone and the black area to the burned zone. Point ignition occurs at $x = 150\delta l$ and $y = 0$. $l_x = 2\delta l$, $l_y = 6\delta l$, $t_{\mathrm{TD}} = 100\delta t$, and $t_{\mathrm{c}} = 30\delta t$.

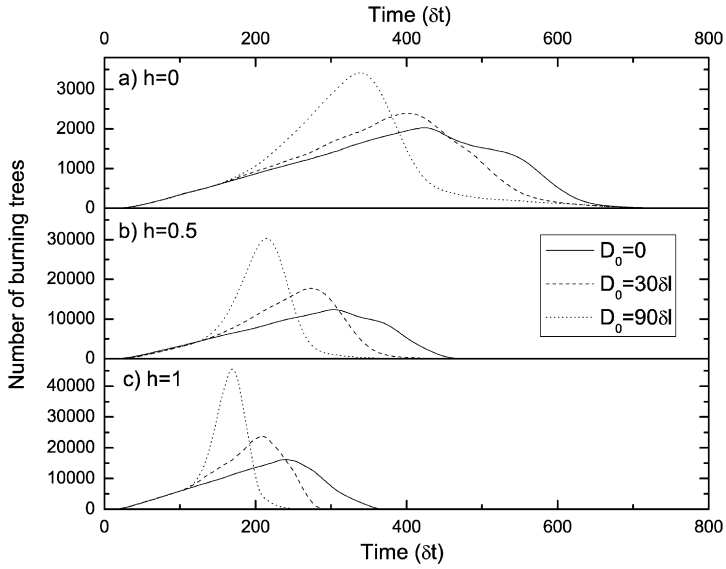

Fig. 15. Time evolution of the number of burning sites for nonspotting and spotting fire propagations with characteristic spotting distances $D_0 = 30$ and $90\delta l$, and (a) $h = 1$, (b) $h = 0.5$, and (c) $h = 0$. Diagrams (b) and (c) correspond to 50% of inactive sites. $l_x = 2\delta l$, $l_y = 6\delta l$, $t_{\mathrm{TD}} = 100\delta t$, and $t_{\mathrm{c}} = 30\delta t$.

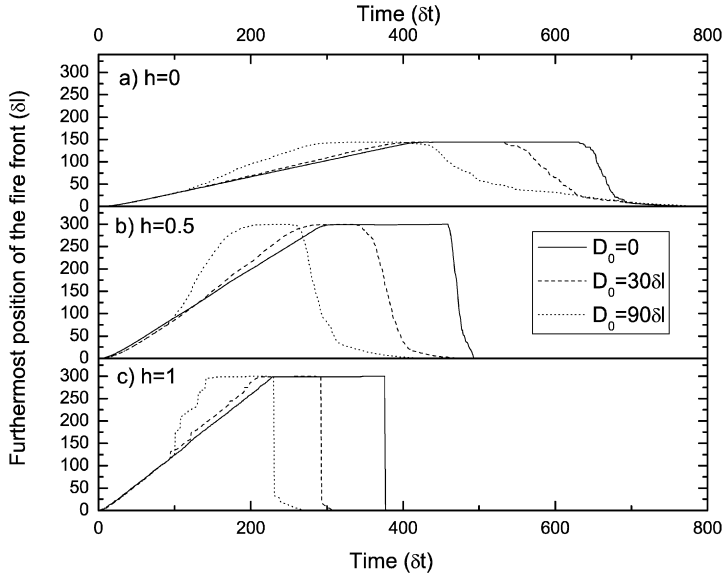

Fig. 16. Time evolution of the furthermost position of the fire front for nonspotting and spotting fire propagations with characteristic spotting distances $D_0 = 30$ and $90\delta l$, and (a) $h = 1$, (b) $h = 0.5$, and (c) $h = 0$. Diagrams (b) and (c) correspond to 50% of inactive sites. $l_x = 2\delta l$, $l_y = 6\delta l$, $t_{\mathrm{TD}} = 100\delta t$, and $t_{\mathrm{c}} = 30\delta t$.

there exist critical links (singly connected links) in the largest cluster [4,41]. Such connections are widened by the contribution of the influence zone. If such critical channels are cut by fire retardants or water, fire cannot spread. This shows that the swn model could be used to optimize the amounts of retardants and water in firefighting strategy and tactics. We show in Fig. 17 a particular configuration where the action of firebrands cause the fire to stop after cutting a critical channel.

4. Conclusion

A weighted-site small world network is used to model forest fire spread. The weighting procedure is

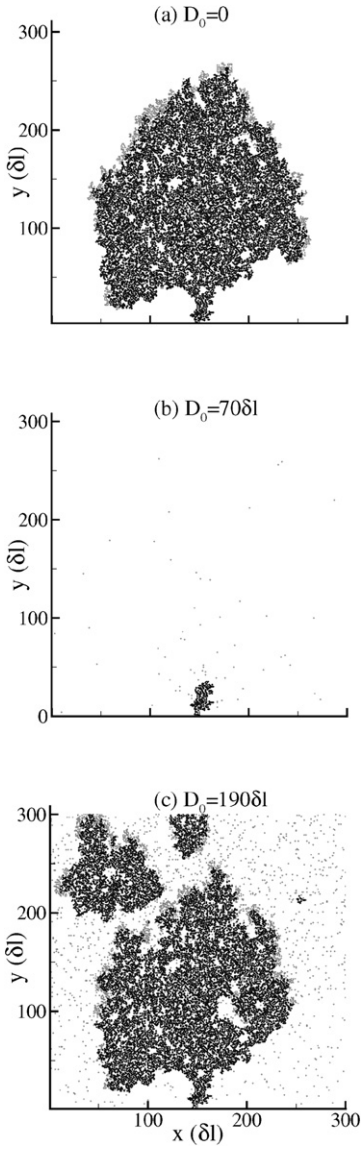

Fig. 17. Fire patterns for nonspotting and spotting fire propagations: (a) $D_0 = 0$, (b) $D_0 = 70\delta l$, and (c) $D_0 = 190\delta l$. The density of active sites is $p = 0.38$; the impact parameters are $l_x = 2\delta l$ and $l_y = 4\delta l$. $t_{TD} = 100\delta t$ and $t_c = 30\delta t$. Note that for case (b) propagation stops due to the cutting of a critical channel by firebrands.

based on the physical concepts of thermal degradation and combustion of vegetation elements. Long-range connections correspond to firebrands, whereas short-range connections are related to the fire impact zone. The following conclusions may be drawn.

For nonspotting systems:

- Applied to homogeneous systems, the present model satisfactorily reproduces the time evolution of the fire perimeter and the nonlinear behavior of the ros as wind speed increases, as observed in experiments. Its application to heterogeneous systems shows the complex patterns formed for more realistic situations when the fire and fuel conditions vary in space. Furthermore, the density of active (flammable) sites, p, seems to be a good measure of the swn effect on fire propagation.
- With a computational time significantly smaller than real time, the present model can then be considered as the base of an operational tool for fire fighting management as well as a training tool for firefighters.
- This model exhibits geometric and dynamic propagation thresholds. The former is a second-order phase transition line and is inversely proportional to the impact parameter, according to $p_c^{rn} = 0.5 l_c^{-1}$. The dynamic threshold results from the weighting procedure.
- The sharp variation of the fractal dimension as a function of p at the percolation threshold can be used to determine the numerical value of p_c^{rn}.
- Two regimes appear: the ballistic regime for a system whose size is smaller than the influence zone and the diffusive regime for large systems. For the former the swn effect is dominant, whereas the regular network effect dominates for the latter. The crossover between these two regimes is studied.

For spotting systems:

- For homogeneous systems, the action of firebrands is all the more pronounced since the impact parameter is small and the spotting distance is large (spotfires have enough time to develop before being caught up by the primary fire front).
- When the size of the system is finite and smaller than the spotting distance, the probability of emission of efficient firebrands within the system becomes size-dependent. At the thermodynamic limit (infinite-size systems), this probability becomes constant and equal to c, calculated from Eq. (3).
- For heterogeneous systems, the degree of heterogeneity reduces the action of efficient firebrands on fire propagation.
- For a completely heterogeneous system, saturation of the spotting effect is expected during propagation when the largest cluster size is smaller than D_0.
- Around the regular network percolation threshold, critical channels appear. If such channels are cut (e.g., using fire inhibitors), the fire cannot spread.

This model can also provide a tool for determining the mass involved in fire propagation as a function of p as well as the critical concentration of flammable sites delimiting the spreading/nonspreading transition. This can answer questions about the partial clearance of vegetation, about the efficiency of fuel break, and about house distribution in wildland–urban interface areas. As a consequence of the existence of a second-order phase transition, further studies of the scaling effects and critical exponents near the transitions will be the subject of a forthcoming work.

Acknowledgments

Professors P.G. de Gennes and E. Guyon are gratefully acknowledged for insightful discussions on this problem. This work was supported by the CNRS/DEF n° 17937 and the Ministère de la Recherche (ERT Feux).

References

[1] G. Albinet, G. Searby, D. Stauffer, J. Phys. 47 (1986) 1–7.
[2] J. Nahmias, H. Téphany, E. Guyon, Rev. Phys. Appl. 24 (1989) 773–777.
[3] J. Nahmias, H. Téphany, J.A.M.S. Duarte, C.R. Acad. Sci. II 322 (1996) 113–119.
[4] D. Stauffer, A. Aharony, Introduction to Percolation Theory, Taylor & Francis, London, 1991.
[5] H. Téphany, J. Nahmias, J.A.M.S. Duarte, Physica A 242 (1997) 57–69.
[6] J. Margerit, O. Séro-Guillaume, Proc. Congr. Mech. 13 (1997) 235–238.
[7] G.L. Ball, D.P. Guertin, Int. J. Wildland Fire 2 (1992) 47–54.
[8] F.J. Barros, M.T. Mendes, Simul. Practice Theory 5 (1997) 185–197.
[9] P.G. de Gennes, La Recherche 7 (1976) 919–927.
[10] J.A.M.S. Duarte, in: D. Stauffer (Ed.), Annual Reviews of Computational Physics, World Scientific, Singapore, 1997, p. 1.
[11] D.J. Watts, S.H. Strogatz, Nature 393 (1998) 440–442.
[12] N. Zekri, J.P. Clerc, Phys. Rev. E 64 (2001) 056115.
[13] N. Zekri, J.P. Clerc, C.R. Phys. 3 (2002) 741–747.
[14] M.E.J. Newman, D.J. Watts, Phys. Lett. A 263 (1999) 341–346.
[15] M.E. Newman, D.J. Watts, Phys. Rev. E 60 (1999) 7332–7342.
[16] A. Barrat, M. Barthelemy, R. Pastor-Satorras, A. Vespignani, Proc. Natl. Acad. Sci. USA 101 (2004) 3747–3752.
[17] P.J. Pagni, Fire Safe. J. 21 (4) (1993) 331–340.
[18] C.S. Tarifa, P.P. Del Notario, F.G. Moreno, A.R. Villa, Transport and Combustion of Firebrands, U.S. Dept. of Agriculture Forest Service, Final Report of GRANTS FG-SP-114 and FG-SP-146, Madrid, 1967.
[19] C.S. Tarifa, P.P. Del Notario, F.G. Moreno, Proc. Combust. Inst. 10 (1965) 1021–1037.
[20] F.A. Albini, Combust. Flame 32 (1983) 277–288.
[21] A. Muraszew, J.B. Fedele, W.C. Kuby, Combust. Flame 30 (1977) 321–324.
[22] S.D. Tse, A.C. Fernandez-Pello, Fire Safe. J. 30 (1998) 333–356.
[23] J.P. Woycheese, P.J. Pagni, Int. Conf. Fire Res. Eng., Boston, 1998.
[24] W.W. Hargrove, R.H. Gardner, M.G. Turner, W.H. Romme, D.G. Despain, Ecol. Modelling 135 (2000) 243–263.
[25] B. Porterie, S. Nicolas, J.L. Consalvi, J.C. Loraud, F. Giroud, C. Picard, Numer. Heat Transfer 47 (2005) 471–489.
[26] B. Porterie, N. Zekri, J.P. Clerc, J.C. Loraud, C.R. Phys. 6 (2005) 151–157.
[27] N. Zekri, B. Porterie, J.P. Clerc, J.C. Loraud, Phys. Rev. E 71 (2005) 046121.
[28] http://www.ffp.csiro.au/nfm/fbm/vesta/spotfire.html.
[29] N. Sardoy, J.L. Consalvi, B. Porterie, J.C. Loraud, JITH2005, Tangiers (2005).
[30] P.L. Andrews, C.H. Chase, BEHAVE: Fire Behavior Prediction and Fuel Modeling System—BURN Subsystem, Part 2, National Wildfire Coordinating Group Publication PMS 439-3, NFES 277, 1989.
[31] J.P. Clerc, G. Giraud, J.M. Luck, Adv. Phys. 39 (3) (1990) 191–309.
[32] J.M.C. Mendes-Lopes, J.M.P. Ventura, J.M.P. Amaral, Int. J. Wildland Fire 12 (2003) 67–84.
[33] J.L. Dupuy, Int. J. Wildland Fire 5 (1995) 153–164.
[34] A.A. Putnam, Proc. Combust. Inst. 10 (1965) 1039–1046.
[35] F.A. Albini, Combust. Flame 43 (1981) 155–174.
[36] B. Porterie, D. Morvan, J.C. Loraud, M. Larini, Phys. Fluids 12 (2000) 1762–1782.
[37] B. Sapoval, M. Rosso, J.F. Gouyet, J. Phys. Lett. 46 (1985) L149.
[38] K. Chen, P. Bak, Phys. Rev. E 62 (2000) 1613–1616.
[39] R.M. Anderson, R.M. May, Infectious Diseases of Humans, Dynamics and Control, Oxford Univ. Press, London, 1991.
[40] G. Caldarelli, R. Frondini, A. Gabrielli, M. Montuori, Europhys. Lett. 56 (4) (2001) 510–516.
[41] A. Coniglio, Phys. Rev. Lett. 46 (1981) 250–253.